A Principal Component Based Haze Masking Method for Visible Images

Huifang Li, Liangpei Zhang, *Senior Member, IEEE*, and Huanfeng Shen, *Senior Member, IEEE*

***Abstract*—Land surfaces are commonly obstructed by haze in remote sensing images, which reduces the available land cover information. Haze detection is therefore important for locating, avoiding, or restoring hazy regions. In this letter, a principal component (PC)-based haze masking (PCHM) method is developed for the masking of haze in visible remote sensing images covering land surfaces at middle latitudes. Owing to the evidence of haze in the second PC, the PCHM method results in accurate haze masks. The complete procedure comprises two steps: haze construction and spatial optimization. The validity of the PCHM method is demonstrated through its application to several hazy visible images clipped from Landsat Enhanced Thematic Mapper Plus scenes. The quantitative assessments verify the superiority of the proposed method over the haze optimized transformation method for the production of binary haze masks. In addition, the resulting haze masks are compared with a MODIS cloud product, which further proves the necessity and validity of the proposed method.**

***Index Terms*—Haze masking, principal component (PC), spatial optimization, visible remote sensing images.**

I. Introduction

MOST archived remote sensing images are affected by cloud or haze, which obstructs land surface information. Haze refers to the spatially varying semitransparent cloud and aerosol layer [1]. A variety of atmospheric particles, including water droplets, ice crystals, or fog/smog particles, can form haze [2]. Hereafter, opaque atmospheric layers are referred to as "thick cloud," semitransparent atmospheric layers, including thin clouds, are referred to as "haze," and "cloud" is a general concept covering both thick cloud and haze.

Thick cloud usually shows evident characteristics, such as high reflectance, low temperature [3]–[5], and the presence of shadows [6]–[8]. However, these characteristics are not evident for haze. Haze is transparent, vague, and is without evident boundaries and accompanying shadow; the signal of hazy pixels includes both haze and the surface underneath [9], [10]. According to the low contrast of hazy regions, Du *et al.* [11] suggested that haze is distributed in the low-frequency layer, and in their study, they used wavelet analysis to decompose a hazy image. However, the low-frequency layer might also contain a component of the land cover. Thus, a single-scene-based haze masking method is introduced in this letter, but the application is limited to ice/snow-free scenes.

Zhang *et al.* [1] proposed an image transformation to characterize the haze spatial distribution in Landsat scenes, which is named the haze optimized transformation (HOT). HOT is based on the high sensitivity of the spectral response to both the optical wavelength and the haze optical depth. It is a supervised procedure that requires the assistance of clear pixels.

The automated cloud-cover assessment (ACCA) algorithm designed for Landsat data provides the percentage of clouds in a single FOV, but no cloud map is available [12], [13]. Furthermore, the ACCA score ignores the thin cirrus and haze in the FOV; therefore, it usually underestimates the cloud amount [7]. The Moderate-resolution Imaging Spectroradiometer (MODIS) cloud product (MOD35) is generated by thresholding on 19 visible and infrared channels [3]; however, the spatial resolution is too coarse to mask regional and light haze. There is a need to explore a method for masking haze in images with a moderate (10–100 m) or high (less than 10 m) spatial resolution [14]. Moreover, the infrared channels, such as the near infrared (0.75–1.4 μm) and thermal infrared (8–13 μm) channels, are usually absent in sensors with high spatial resolutions [15]. The detection methods, depending on infrared channels, are therefore not suitable for high-spatial-resolution imagery and some moderate-resolution imagery. Therefore, in this letter, we intend to develop an unsupervised haze masking method by using only the visible channels.

The visible channels are highly correlated, and haze can be easily confused with land surfaces in all these channels. Thus, a space is sought to separate the clear surfaces and haze. It is known that the principal component (PC) space is a typical orthogonal space. In fact, we find that haze shows higher brightness than clear surfaces in some PCs in a scene that is located at middle latitudes. Furthermore, in order to generate haze masks with high accuracy, the spatial characteristics of haze are also considered. A PC-based haze masking (PCHM) method is therefore developed by combining the spectral and spatial features for visible images. It is noted that there are two limitations for the proposed PCHM method: 1) it is only suitable for locally regional haze masking, where "locally" means that there must be clear surfaces existing in the scene and "regional" means that the scene with a moderate or high spatial resolution is not very large, which usually covers an area of less than 1000 km^2; and 2) it only works in ice/snow-free regions that are located in a middle latitude.

Manuscript received July 10, 2013; revised August 29, 2013; accepted September 22, 2013. This work was supported in part by the National Key Basic Research Program of China (973 Program) under Grant 2011CB707103, by the National Natural Science Foundation of China under Grant 40930532 and Grant 41271376, and by the Hubei Natural Science Foundation under Grant 2011CDA096.

H. Li and H. Shen are with the School of Resource and Environmental Science, Faculty of Sciences, Wuhan University, Wuhan 430079, China (e-mail: l.huifang10@gmail.com; shenhf@whu.edu.cn).

L. Zhang is with the State Key Laboratory of Information Engineering in Surveying, Mapping and Remote Sensing, Wuhan University, Wuhan 430079, China (e-mail: zlp62@whu.edu.cn).

Color versions of one or more of the figures in this paper are available online at http://ieeexplore.ieee.org.

Digital Object Identifier 10.1109/LGRS.2013.2283792

(a)

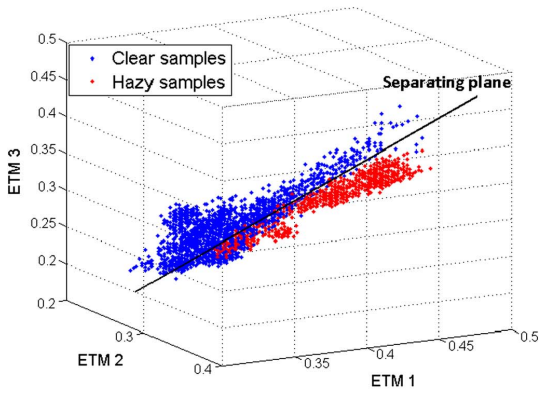

(b)

Fig. 1. (a) Hazy image clipped from an ETM+ scene. (b) Samples in the RGB space and the separating plane between the hazy and clear pixels.

Section II illustrates the PCHM method in detail. In Section III, we take Landsat images to verify the effectiveness of the proposed method, and the results are compared with the HOT results and the MODIS cloud product (i.e., MOD35). Section IV concludes this letter.

II. PCHM Method

The haze reflectance is mainly attributed to the atmospheric scattered energy, which is very sensitive to the wavelength. In the visible spectrum, the scattered energy of the red light is less than that of the blue light; therefore, the images in the red channels show clearer edges than those in the blue channels.

Fig. 1(a) shows a hazy image that is clipped from an Enhanced Thematic Mapper Plus (ETM+) scene, with the true color composed of the first three channels, i.e., the ETM1 (0.48 μm), the ETM2 (0.56 μm), and the ETM3 (0.66 μm). The hazy pixels that are located on the northwest side of the lakes show higher brightness than the surrounding pixels. We manually select the hazy and clear pixel samples from Fig. 1(a) and plot them in the RGB space that is composed of the ETM3, the ETM2, and the ETM1, as shown in Fig. 1(b). The hazy and clear samples can be separated by a plane in the 3-D RGB space, and the separating plane intersects each axis of the RGB space in Fig. 1(b). This indicates that the hazy and clear pixels cannot be well separated in any single visible channel. Considering the differences of the atmospheric scattering in each channel, it is reasonable to suppose that there exists a new space in which the hazy and clear pixels can be well separated.

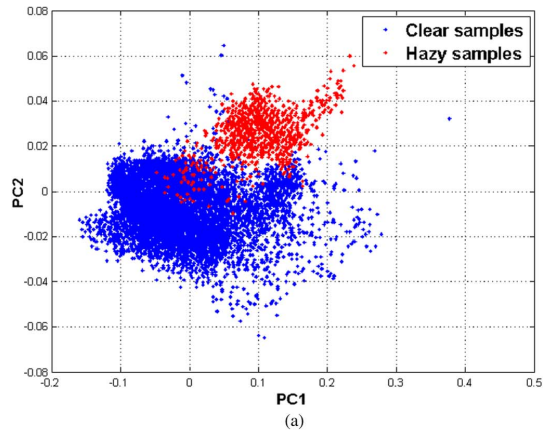

(a)

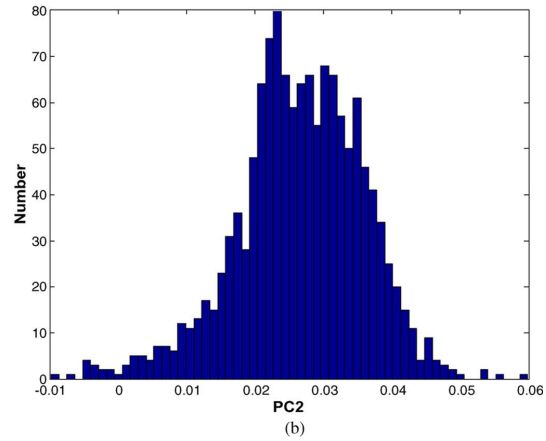

(b)

Fig. 2. (a) Scatter plot of the samples in the PC1–PC2 space. (b) Histogram of the hazy samples in PC2.

In the transformed orthogonal space, significant information is preserved in the first few PCs, and noise and trivial information are left in the other components. The following section will discuss the effect of the PC transformation for the separation of hazy and clear pixels [16].

A. PCs of Hazy Visible Imagery

Denote a data matrix $\mathbf{X}_{m\times n}$ with $\boldsymbol{n}$ samples and $\boldsymbol{m}$ components, and the centralized matrix with a zero mean of $\mathbf{X}$ is $\bar{\mathbf{X}}$. Suppose the transform matrix is $\mathbf{P}$, the formulation of the PC transformation can be written as

$$\mathbf{Y} = \mathbf{P}\bar{\mathbf{X}}. \tag{1}$$

The selected hazy and clear samples are plotted in the orthogonal space that is composed of the first and second components, which is named the PC1–PC2 space, as shown in Fig. 2(a). Clearly, almost all of the hazy samples have positive values in PC2, and thus, they are located at the top of the PC1–PC2 plane, whereas the clear samples are located at the bottom of the plane. Fig. 2(b) shows the histogram of the hazy samples in PC2, which indicates that more than 95% of the hazy samples are positive in PC2. This suggests that the hazy pixels are enhanced, whereas the clear pixels are suppressed in PC2, which indicates that they are separable in this axis.

Visually, for a locally regional hazy image, the land surface information dominates the image, but the influence of haze on each channel is evident.

Quantitatively, (2) shows the transformation matrix $\mathbf{P}$ of the test image shown in Fig. 1(a). The columns of $\bar{\mathbf{X}}$ represent the blue, green, and red channels, respectively, and the elements in each row of $\mathbf{P}$ weigh these three channels in the corresponding component. It can be observed that the red channel makes the biggest contribution to PC1, the blue channel makes the biggest contribution to PC2, and the weight of the red channel in PC2 is negative. Correspondingly, the atmospheric scattering in the blue channel is the most severe of the three channels, which suggests that the radiation increase due to haze in the blue channel is the highest. This explains why haze is enhanced in PC2

$$\mathbf{P} = \begin{bmatrix} 0.37 & 0.48 & 0.80 \\ 0.80 & 0.28 & -0.54 \\ -0.48 & 0.83 & -0.28 \end{bmatrix}. \tag{2}$$

The HOT method, as used for detecting haze, is expressed as

$$\text{HOT} = \text{TM}_1 \sin\theta - \text{TM}_3 \cos\theta \tag{3}$$

where θ is the slope angle of the clear line, which is a well-defined surface response vector under clear atmospheric conditions in the spectral space that is composed of the first (blue) and third (red) channels of a Landsat TM image.

Comparing (2) and (3), it can be found that PC2 and HOT are consistent in essence. The difference is that $\mathbf{P}$ is calculated from the whole image, whereas θ is estimated from selected clear samples. The former is an unsupervised procedure, and the latter is a supervised procedure.

B. PCHM Method

Due to the separability of the hazy and clear pixels in PC2, the PCHM method is proposed. It consists of two steps: the haze base construction, which is based on PC2 and the original spectral features, and the haze mask optimization, which takes some spatial features into consideration. Three filters are contained in the first step and two in the second step. Here, a filter refers to a thresholding procedure rather than a traditional spatial or frequential filter.

a) Haze Base Construction: The haze base refers to a gray or binary image in which all the hazy pixels are enhanced or marked. It is a coarse haze mask, in which some false hazy pixels may be confused. Three filters are included in this step.

1) PC filter PC2: The PC transformation is executed on the input hazy image that is composed of the three visible channels. Due to the good separability of the hazy and clear pixels, as verified before, PC2 is taken as the first filter criterion. Pixels with positive values in PC2 are all considered hazy candidates, and the others are marked as clear pixels. This procedure results in a gray image $T(\text{PC2})$, in which the hazy candidates reserve their values in PC2, and the other pixels are 0.

2) Blue target filter $Rblue\_level$: As aforementioned, the blue channel contributes the most in the calculation of PC2. Thus, blue targets, such as blue buildings and some lakes, show high brightness, which is similar to the hazy pixels in PC2, and should be excluded from the final hazy pixels. For the blue targets, their mean radiation in the three visible channels is usually lower than that of the hazy pixels. Therefore, the ratio of PC2 and the mean radiation of the three channels mI can be taken as a criterion to exclude the blue targets.

Here, in order to unify the data range and avoid the issue of setting different thresholds, we use Otsu's automatic multithresholding method [17] to segment the given variables to certain levels. Thus, mean radiation mI is first segmented to five levels, and the result is rating image mI_level whose dynamic range is [1, 5]. The ratio $Rblue$ for excluding the blue targets is then obtained by

$$Rblue = T(\text{PC2})/mI\_level. \tag{4}$$

As with the mean radiation, $Rblue$ is segmented to six levels, which is written as $Rblue\_level$. Pixels with $Rblue\_level$ values larger than 3 or 4 in our experiments are considered clear blue targets and false hazy pixels. Binary image $B(Rblue\_level)$ is the result of this filter, in which the clear blue targets are labeled 0 and the others 1.

3) Man-made object filter $Ired\_level$: Other than the blue targets, another factor that causes commission error is man-made objects such as buildings, roads, etc. These objects usually have high radiation values, as with the hazy pixels. The key difference is that man-made objects usually have extremely high radiation in the red channel, whereas the atmospheric scattering in the red channel is the weakest in the three visible channels; therefore, the radiation values of hazy pixels in the red channel are moderate. Thus, the radiation in the red channel is taken as another criterion to exclude false hazy pixels. As with the blue target filter, we segment the radiation of an image in the red channel into four levels, and the pixels with values larger than 3 are considered clear man-made objects, whereas the others are marked as hazy pixels. Binary image $B(Ired\_level)$ is the result of this filter, in which clear man-made objects are labeled 0 and the others 1.

Integrating the given three filters and the spectral features, the haze base can be expressed as

$$Haze\ Base = [mI\_level \cdot T(\text{PC2}) \cdot B(Rblue\_level) \cdot B(Ired\_level)] > 0. \tag{5}$$

The $HazeBase$, which resulted from Step 1 of the algorithm that is reported in the following, is a binary mask, with hazy candidates marked as 1 and the clear pixels marked as 0.

Step 1: Haze base construction

Input: visible imagery with three channels.
Require: PCs PCi($i = 1, 2, 3$),
segmented mean radiance mI_level,
ratio $Rblue$, segmented ratio $Rblue\_level$,
and segmented red radiance $Ired\_level$.
1: if PC2 > 0 then $T(\text{PC2}) = \text{PC2}$;
else $T(\text{PC2}) = 0$, output clear pixels.
2: if $Rblue\_level \leq 4$ or 3 then $B(Rblue\_level) = 1$;
else $B(Rblue\_level) = 0$, output clear blue targets.
3: if $Ired\_level \leq 3$ then $B(Ired\_level) = 1$;
else $B(Ired\_level) = 0$, output clear man-made objects.
Output: a primary binary haze mask:

$$Haze\ Base = [mI\_level \cdot T(\text{PC2}) \cdot B(Rblue\_level) \cdot B(Ired\_level)] > 0$$

b) Spatial Optimization: In the obtained haze base, almost all the hazy pixels are extracted, and most of the false hazy pixels are excluded. However, it is inevitable that there will still be some minor targets that are confused with the hazy candidates. Hence, spatial optimization is performed to refine the haze mask, in which two filters are included.

4) Area filter: Haze is a type of a macroscopic atmospheric condition, which usually covers tens of thousands of square meters. In a moderate resolution satellite image, objects with areas of less than 100 pixels are removed from the haze base, and the others are left.

5) Shape filter: Haze is usually an area object rather than a linear or point object. Here, the bounding ellipse of an object, which has the same normalized second central moments as the object, is taken as the criterion to measure its shape. For an area object, the ratio R_{ab} of the minor and major axis lengths of the ellipse and the minor axis length b should not be too small. In our experiments, objects with R_{ab} values of less than 0.2, or b values of less than 10, are considered clear narrow objects, such as roads or river banks.

Almost all the hazy pixels are extracted after the area and shape filters are performed, but haze should be spatially continuous and smooth in a local region. Hence, three operations aiming to ensure the spatial continuity and smoothness follow the two given spatial filters: 1) morphological closing; 2) smoothing by a mean filter; and 3) filling of the image holes.

Step 2: Spatial optimization

Input: the primary binary haze mask $Haze\ Base$
4: if $Area > 100$ then reserve the object; else abandon the object.
5: if $R_{ab} \geq 0.2$ and $b \geq 10$ then reserve the object; else abandon the object.
Postprocessing: morphological closing, smoothing by a mean filter and filling of the image holes.
Output: an optimized binary haze mask.

The procedure of the PCHM method is now complete, and a spatially continuous and smooth haze mask is obtained after the two given steps, i.e., the haze base construction and the spatial optimization, are performed.

III. Experiments

For the experiments, we select six ETM+ images distributed in three different provinces of China, i.e., Jiangxi, Jiangsu, and Hubei, with the latitude ranging from N 24.3° to N 35.3°. Four of the six images are shown in Fig. 3, and the regions that are surrounded by the yellow lines are the detected haze. The first row of Fig. 3 shows the masking results of the proposed PCHM method. The thresholds of the five filters in this method are set following the instructions in Section II. Visually, most of the marked hazy pixels are true and that most of the true hazy pixels are marked. Since no true haze masks are available, the reference masks for the quantitative assessment are generated by manual drawing according to a naked-eye preliminary interpretation. The precision ratio and the recall ratio are taken as measurements and are calculated for these six images, respectively, as listed in Table I. The precision ratios of

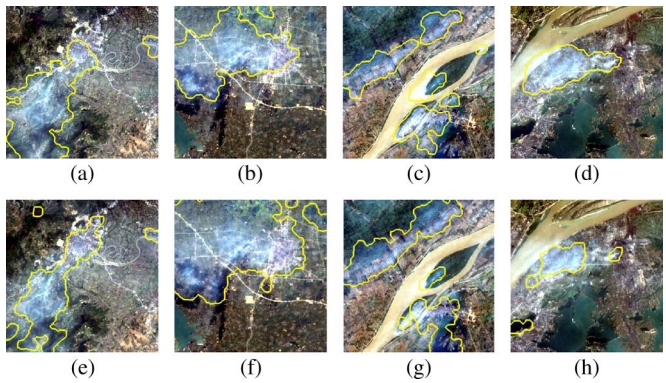

Fig. 3. Four ETM+ images from three different provinces in China. First row: the results of the PCHM method. Second row: the results of the HOTso method. (a) and (e) Number 1 ETM+ image from Jiangxi on March 26, 2003. (b) and (f) Number 2 ETM+ image from Jiangsu on October 8, 2002. (c) and (g) Number 3 image from Hubei on October 13, 2002. (d) and (h) Number 4 ETM+ image from Hubei on October 13, 2002.

TABLE I
Quantitative Assessment Results

No.	Precision ratio (%)		Recall ratio (%)	
	PCHM	HOTso	PCHM	HOTso
1	93.73	85.14	81.57	56.87
2	93.82	65.42	84.09	99.85
3	86.09	71.10	77.75	72.60
4	86.45	77.37	80.97	40.47
5	90.36	79.29	69.85	66.42
6	93.85	73.14	73.20	50.86

the PCHM method are approximately 90%, which verifies the correctness of the results. Moreover, the recall ratios range from 70% to 80%, which confirms the completeness of the results.

As aforementioned in Sections I and II, HOT is an effective supervised haze enhancement method that only uses the visible channels. Hence, we compare the proposed PCHM method with the HOT method through experiments. The HOT method results in a gray image, in which the hazy pixels are enhanced and the others are suppressed, whereas our proposed method results in a binary haze mask. Thus, for comparability, a threshold is first set to binarize the HOT image, and then, the same spatial optimization that is used with the PCHM method is performed on the binary HOT image. The spatially optimized binary HOT (HOTso) results are shown in the second row of Fig. 3. Visually, some obvious hazy pixels are missed. Moreover, clear forests and lakes are wrongly marked as haze in Fig. 3(a) and (e) and Fig. 3(d) and (h). This can be attributed to the high radiation values of the clear forests and lakes in the blue channel, and HOT does not remove them from the hazy candidates. The precision ratios and the recall ratios are also calculated and listed in Table I. It should be noted that the recall ratio of Fig. 3(f) is high at 99.85%, but the precision ratio is only 65.42%. This is because Fig. 3(f) is an overestimation of the true haze. Overall, the PCHM method outperforms the HOTso method according to both the visual and quantitative assessments.

The result of the PCHM method is compared with the MODIS cloud product as follows. Fig. 4(a) shows a MODIS FOV covering Hubei, which is observed on the same day as the ETM+ scene shown in Fig. 4(b). The cloud confidence mask based on bits 1 and 2 is shown in Fig. 4(c), and the enlargement of Hubei is shown in Fig. 4(d). It is shown that most pixels are marked as confident clear, the Yangtze River

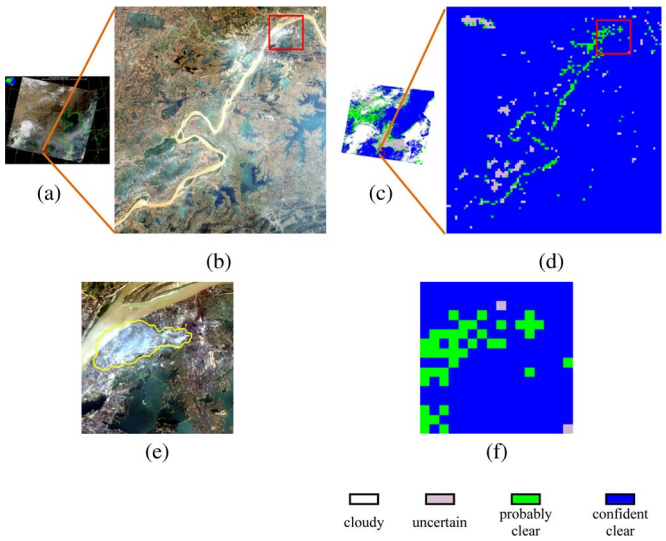

Fig. 4. Comparison between the PCHM result and the MODIS product. (a) MODIS FOV. (b) ETM+ scene that is located in Hubei. (c) MODIS cloud mask product with four levels. (d) Corresponding MODIS cloud mask in Hubei. (e) ETM+ image that is located in Wuhan. (f) Corresponding MODIS cloud mask in Wuhan.

basin is marked as probably clear, and some vegetation regions are incorrectly marked as uncertain. Furthermore, the evident haze that is located in Wuhan, which is the capital city of Hubei, as shown in Fig. 4(e), is missed in Fig. 4(f). Moreover, both bits 9 and 11 flag all the pixels in Hubei as clear, and as such, they are not shown in the figures. The MODIS product, therefore, cannot be applied to the thin cloud detection in a province or a city region. Fig. 4(e) is the detection result of the proposed PCHM method, whose precision ratio is 86.45% and whose recall ratio is 80.97%. This suggests that the PCHM method that uses only the visible channels can result in satisfactory haze masks in a city region.

IV. Conclusion

The PCHM method has been developed for use with visible remote sensing images. Two steps are included: the haze base construction and the spatial optimization. In the first step, three filters are used to screen the hazy pixels. A binary base with all possible hazy pixels marked is obtained from the first step. In the second step, the remaining nonhazy pixels are first effectively removed by using two spatial filters, which are according to the area and shape. Morphological closing, smoothing by the mean filter, and the filling of the holes are then executed to obtain the final spatially continuous and smooth haze mask.

ETM+ images were employed to verify the proposed PCHM method, and the experimental results suggest that the PCHM method can effectively yield haze masks with a satisfactory correctness and completeness from both the visual and quantitative assessments. Furthermore, the comparative analysis shows that the PCHM method outperforms HOT in the resulting binary hazy masks, and the MODIS product is too coarse to mark locally regional haze. Exploring the extension of the PCHM method on images with high resolutions and finding an adaptive way to tune some empirical thresholds will be the subject of our future work.

References

[1] Y. Zhang, B. Guindon, and J. Cihlar, "An image transform to characterize and compensate for spatial variations in thin cloud contamination of Landsat images," *Remote Sens. Environ.*, vol. 82, no. 2/3, pp. 173–187, Oct. 2002.

[2] Y. J. Kaufman, *The Atmospheric Effect on Remote Sensing and Its Correction*. New York, NY, USA: Wiley, 1989.

[3] S. A. Ackerman, K. I. Strabala, W. P. Menzel, R. A. Frey, C. C. Moeller, and L. E. Gumley, "Discriminating clear sky from clouds with MODIS," *J. Geophys. Res. D—Atmos.*, vol. 103, no. 24, pp. 32 141–32 157, Dec. 1998.

[4] R. R. Irish, "Landsat 7 automatic cloud cover assessment," in *Proc. SPIE*, Orlando, FL, USA, 2000, pp. 348–355.

[5] R. R. Irish, J. L. Barker, S. N. Goward, and T. Arvidson, "Characterization of the Landsat-7 ETM automated cloud-cover assessment (ACCA) algorithm," *Photogramm. Eng. Remote Sens.*, vol. 72, no. 10, pp. 1179–1188, 2006.

[6] H. Choi and R. Bindschadler, "Cloud detection in Landsat imagery of ice sheets using shadow matching technique and automatic normalized difference snow index threshold value decision," *Remote Sens. Environ.*, vol. 91, no. 2, pp. 237–242, May 2004.

[7] Z. Zhu and C. E. Woodcock, "Object-based cloud and cloud shadow detection in Landsat imagery," *Remote Sens. Environ.*, vol. 118, pp. 83–94, Mar. 2012.

[8] N. R. Goodwin, L. J. Collett, R. J. Denham, N. Flood, and D. Tindall, "Cloud and cloud shadow screening across Queensland, Australia: An automated method for Landsat TM/ETM+ time series," *Remote Sens. Environ.*, vol. 134, pp. 50–65, Jul. 2013.

[9] R. Richter, "Atmospheric correction of satellite data with haze removal including a haze/clear transition region," *Comput. Geosci.*, vol. 22, no. 6, pp. 675–681, Jul. 1996.

[10] Q. Li, W. Lu, J. Yang, and J. Z. Wang, "Thin cloud detection of all-sky images using Markov random fields," *IEEE Geosci. Remote Sens. Lett.*, vol. 9, no. 3, pp. 417–421, May 2012.

[11] Y. Du, B. Guindon, and J. Cihlar, "Haze detection and removal in high resolution satellite image with wavelet analysis," *IEEE Trans. Geosci. Remote Sens.*, vol. 40, no. 1, pp. 210–217, Jan. 2002.

[12] P. L. Scaramuzza, M. A. Bouchard, and J. L. Dwyer, "Development of the landsat data continuity mission cloud-cover assessment algorithms," *IEEE Trans. Geosci. Remote Sens.*, vol. 50, no. 4, pp. 1140–1153, Apr. 2012.

[13] *NASA, Landsat 7 Science Data Users Handbook*, NASA, Washington, DC USA, 2006.

[14] F. Gao, J. G. Masek, R. E. Wolfe, and C. Huang, "Building a consistent medium resolution satellite data set using moderate resolution imaging spectroradiometer products as reference," *J. Appl. Remote Sens.*, vol. 4, no. 1, pp. 043526-1–043526-22, 2010.

[15] M. S. Alam, J. G. Bognar, R. C. Hardie, and B. J. Yasuda, "Infrared image registration and high-resolution reconstruction using multiple translationally shifted aliased video frames," *IEEE Trans. Instrum. Meas.*, vol. 49, no. 5, pp. 915–923, Oct. 2000.

[16] I. Jolliffe, *Principal Component Analysis. Online Library*. New York, NY, USA: Wiley, 1990.

[17] N. Otsu, "A threshold selection method from gray-level histograms," *Automatica*, vol. 11, no. 285–296, pp. 23–27, 1975.